

Active Bucketized Learning for ACOPF Optimization Proxies

Michael Klamkin, Mathieu Tanneau, Terrence W.K. Mak, Pascal Van Hentenryck

School of Industrial and Systems Engineering
Georgia Institute of Technology
Atlanta, GA, USA

{mklamkin, mathieu.tanneau, wmak, pvh}@gatech.edu

Abstract

This paper considers optimization proxies for Optimal Power Flow (OPF), i.e., machine-learning models that approximate the input/output relationship of OPF. Recent work has focused on showing that such proxies can be of high fidelity. However, their training requires significant data, each instance necessitating the (offline) solving of an OPF for a sample of the input distribution. To meet the requirements of market-clearing applications, this paper proposes Active Bucketized Sampling (ABS), a novel active learning framework that aims at training the best possible OPF proxy within a time limit. ABS partitions the input distribution into buckets and uses an acquisition function to determine where to sample next. It relies on an adaptive learning rate that increases and decreases over time. Experimental results demonstrate the benefits of ABS.

1 Introduction

The *AC Optimal Power Flow* (ACOPF) is a core building block in power systems that finds the most economical generation dispatch meeting the load demand, while satisfying the physical and operational constraints of the underlying systems. The problem is used in many applications, ranging from day-ahead security-constrained unit commitment (SCUC) (Sun et al. 2017), real time security-constrained economic dispatch (SCED) (Tam 2011), transmission switching optimization (Fisher, O’Neill, and Ferris 2008), capacitor placement problems (Baran and Wu 1989), and expansion planning (Verma, Mukherjee et al. 2016).

The non-convexity of ACOPF limits the solving frequency of many operational tools. In practice, generation schedules in real time markets are required to be updated every 5 - 15 minutes, varying from region to region. With the continuous integration of renewable energy sources and demand response mechanisms to meet renewable targets, load and generation uncertainties are expected to be more and more severe. Solving generation schedules using historical forecasts may no longer be optimal, and may not even be feasible in the worst case. Balancing generation and load rapidly without sacrificing economical efficiency is thus an important challenge.

Recently, an interesting line of research has focused on how to learn and predict ACOPF using optimization proxies, such as Deep Neural Networks (DNN) (Fioretto, Mak,

and Van Hentenryck 2020; Yan and Xu 2020; Pan, Zhao, and Chen 2019). Once a DNN model is trained, predictions can be computed in milliseconds. Preliminary results are encouraging, indicating that DNNs can predict ACOPF solutions with high accuracy. However, most prior work (Tang, Dvijotham, and Low 2017; Diehl 2019; Owerko, Gama, and Ribeiro 2020; Dong et al. 2020; Pan et al. 2020; Zamzam and Baker 2020; Canyasse, Dalal, and Mannor 2017; Baker 2020; Guha et al. 2019; Yu et al. 2012) ignore the computational time spent gathering or sampling ACOPF training data in practice (e.g, on realistic networks with thousands of buses). In particular, when generator commitments and grid topology change from day to day (or even within hours) to respond to wind forecast updates, it becomes impractical to develop a sophisticated learning mechanism that requires hours to sample and solve ACOPF instances. On the other hand, generating data sets and training a generalized framework “once-for-all” for all possible commitments, forecasts, and potential grid topologies is also unlikely to be feasible due to the exponential number of configurations & scenarios of a transmission grid. Therefore, *how to actively generate samples and train a “Just-in-Time” model* (Chen et al. 2022), based on the current and forecasted information, is an important practical question for learning approaches.

This paper studies whether active sampling can address this important issue and, more generally, decrease the resource consumption needed to train optimization proxies. It proposes Active Bucketized Sampling (ABS), a novel active learning framework to perform “Just-in-Time” training. Contrary to many active learning frameworks that generate new samples based on the evaluations of individual (or groups of (Kirsch, Van Amersfoort, and Gal 2019)) unlabeled data samples, ABS reasons about regions of the input distribution, exploiting the fact that similar inputs should generally produce similar outputs. The input distribution is thus bucketized and each bucket is evaluated (using an independent validation set) to determine if it needs additional samples. ABS also uses a novel adjustment scheme for the learning rate, which can both decrease and *increase* appropriately, and examines a variety of acquisition functions for evaluating buckets, inspired by several state-of-the-art approaches, e.g., EMCM, BADGE, and MCDUE. ABS was evaluated on large transmission networks and compared to the state of the art in active sampling. The experimental re-

sults show that ABS produces significant benefits for Just-In-Time training. The contributions of this paper can thus be summarized as follows:

1. The paper proposes ABS, a novel active bucketized learning framework for Just-In-Time learning. Its key novelty is the idea of partitioning the input distribution into buckets to determine which buckets are in need of additional samples. This bucket-based sampling contrasts with existing active learning schemes that determine which unlabelled samples to add based on the evaluation of their individual properties.
2. To determine which buckets are in need of more samples, ABS uses an independent validation set, decoupling the assessment of where new samples are needed from the sample generation. This allows additional flexibility when learning optimization proxies, including the ability to avoid generating too many infeasible problems.
3. The paper studies multiple acquisition functions for ABS, highlighting the benefits of gradient information.
4. ABS uses a new adjustment scheme for the learning rate that may now decrease and *increase*.
5. The paper presents an experimental evaluation of ABS on large ACOPF benchmarks, including the French transmission network, and demonstrates its benefits compared to state-of-the-art approaches.

The rest of the paper is organized as follows. Section 2 presents background materials on ACOPF and active sampling. Section 3 discusses related work on active sampling and ACOPF learning. Section 4 introduces the novel active sampling framework for ACOPF. Section 5 reports experimental evaluations and Section 6 concludes the paper.

2 Background

This section presents the notations, the motivating application, and the background in sampling and active learning.

2.1 Nomenclature

This paper uses calligraphic capitals \mathcal{X} for sets, gothic capitals \mathfrak{X} for distributions, $\text{supp}(\mathfrak{X})$ for the support set of \mathfrak{X} (i.e., points with non-zero probability mass), \bar{y}/\underline{y} for the upper/lower bound of variable y , y^* for the optimal value of y , and \hat{y} for its prediction. \mathbf{x} and \mathbf{y} represent the (flattened) vector of input and output features respectively.

2.2 AC Optimal Power Flow

The AC Optimal Power Flow (ACOPF) aims at finding the most economical generation dispatch to meet load demand, while satisfying both the transmission and operational constraints. The ACOPF is non-linear and non-convex.

Let $\mathcal{P} = \{\mathcal{N}, \mathcal{L}, \mathcal{G}, \mathcal{E}\}$ be a power grid with a set of buses \mathcal{N} , a set of loads \mathcal{L} , a set of generators \mathcal{G} , and a set of transmission branches (lines & transformers) \mathcal{E} . In addition, let $\mathcal{G}(i)$ and $\mathcal{L}(i)$ be the set of generators and loads located on bus i . Model 1 illustrates a simplified formulation (Cain et al. 2012) of ACOPF with the symbol descriptions listed in Table 1. Objective (1.1) minimizes the generation costs $c_i : \mathbb{R}^{|\mathcal{G}|} \mapsto \mathbb{R}$ for all the generators. Con-

Model 1 AC Optimal Power Flow — ACOPF($\mathbf{p}^d, \mathbf{q}^d$)

$$\min \sum_{i=1}^{|\mathcal{G}|} c_i(\mathbf{p}_i^g) \quad (1.1)$$

$$\text{s.t. } \underline{\mathbf{v}}_i \leq \mathbf{v}_i \leq \bar{\mathbf{v}}_i \quad \forall i \in \mathcal{N} \quad (1.2)$$

$$\underline{\mathbf{p}}_i^g \leq \mathbf{p}_i^g \leq \bar{\mathbf{p}}_i^g \quad \forall i \in \mathcal{G} \quad (1.3)$$

$$\underline{\mathbf{q}}_i^g \leq \mathbf{q}_i^g \leq \bar{\mathbf{q}}_i^g \quad \forall i \in \mathcal{G} \quad (1.4)$$

$$(\mathbf{p}_{ij}^f)^2 + (\mathbf{q}_{ij}^f)^2 \leq \bar{S}_{ij}^2 \quad \forall (i, j) \in \mathcal{E} \quad (1.5)$$

$$\mathbf{p}_{ij}^f = g_{ij} \mathbf{v}_i^2 - \mathbf{v}_i \mathbf{v}_j (b_{ij}) \quad \sin(\theta_i - \theta_j) + g_{ij} \cos(\theta_i - \theta_j) \quad \forall (i, j) \in \mathcal{E} \quad (1.6)$$

$$\mathbf{q}_{ij}^f = -b_{ij} \mathbf{v}_i^2 - \mathbf{v}_i \mathbf{v}_j (g_{ij}) \quad \sin(\theta_i - \theta_j) - b_{ij} \cos(\theta_i - \theta_j) \quad \forall (i, j) \in \mathcal{E} \quad (1.7)$$

$$\sum_{j \in \mathcal{G}(i)} \mathbf{p}_j^g - \sum_{j \in \mathcal{L}(i)} \mathbf{p}_j^d = \sum_{i, j \in \mathcal{E}} \mathbf{p}_{ij}^f \quad \forall i \in \mathcal{N} \quad (1.8)$$

$$\sum_{j \in \mathcal{G}(i)} \mathbf{q}_j^g - \sum_{j \in \mathcal{L}(i)} \mathbf{q}_j^d = \sum_{i, j \in \mathcal{E}} \mathbf{q}_{ij}^f \quad \forall i \in \mathcal{N} \quad (1.9)$$

| Bus i | | Branch (i, j) | |
|------------------|---------------------|---------------------|-----------------------------------|
| \mathbf{p}_i^d | Active demand | \mathbf{p}_{ij}^f | Active power flow |
| \mathbf{q}_i^d | Reactive demand | \mathbf{q}_{ij}^f | Reactive power flow |
| \mathbf{p}_i^g | Active generation | g_{ij} | Conductance |
| \mathbf{q}_i^g | Reactive generation | b_{ij} | Susceptance |
| \mathbf{v}_i | Voltage magnitude | $\Delta\theta_{ij}$ | Phase diff: $\theta_i - \theta_j$ |
| θ_i | Voltage phase angle | | |

Table 1: Symbols for Model 1

straint (1.2) enforces the upper & lower bounds for voltage magnitude \mathbf{v} . Constraints (1.3)-(1.4) impose the active \mathbf{p}^g and reactive \mathbf{q}^g generation bounds. Constraint (1.5) enforces the thermal limits \bar{S}_{ij} on the apparent power for each line. Constraints (1.6)-(1.7) assert Ohm's Law for all the lines. Constraints (1.8)-(1.9) maintain power flow conservation (Kirchhoff's Law) for all the buses. For simplicity, Model 1 skips the detailed equations for bus shunts, transformers, and DC lines. These components are considered and implemented in this work.

2.3 Sampling for OPF

While some prior learning approaches on energy system optimization, e.g., (Tang et al. 2021; Chen et al. 2022), rely on forecast data, many other learning approaches rely on purely random perturbation on input parameters (e.g., the loads at each bus) for their training & testing data sets.

Algorithm 1 shows a random sampling procedure that perturbs load values from a nominal point \mathbf{x}_0 . The algorithm considers both regional influence and individual variations, modeled by the two variation distributions \mathfrak{B} and \mathfrak{C} . Algorithm 1 illustrates a general data generation pipeline commonly found in prior work, e.g., (Pan et al. 2020; Baker 2020; Guha et al. 2019; Owerko, Gama, and Ribeiro 2020;

Algorithm 1 ACOPF Load Perturbation (LOADPERTURB)

```

1: Input: Nominal sample  $\mathbf{x}_0 = (\mathbf{p}^d, \mathbf{q}^d)$ , regional load
   variation distribution  $\mathfrak{B}$ , individual noise variation dis-
   tribution  $\mathfrak{E}$ , and data set size  $n$ .
2:  $\mathcal{D} \leftarrow \{\}$ 
3: for  $i = 1 \dots n$  do
4:    $b_i \sim \mathfrak{B}$ ,  $b_i \in \mathbb{R}^{2|\mathcal{L}|}$ 
5:    $\epsilon_i \sim \mathfrak{E}$ ,  $\epsilon_i \in \mathbb{R}^{2|\mathcal{L}|}$ 
6:    $\mathbf{x}_i \leftarrow b_i \cdot \mathbf{x}_0 + \epsilon_i$ ,  $\mathbf{x}_i \in \mathbb{R}^{2|\mathcal{L}|}$ 
7:    $\mathbf{y}_i \leftarrow (\mathbf{p}^g, \mathbf{q}^g, \mathbf{v}, \boldsymbol{\theta}) \leftarrow \text{ACOPF}(\mathbf{x}_i)$ ,
      $\mathbf{y}_i \in \mathbb{R}^{2|\mathcal{G}|+|\mathcal{N}|+|\mathcal{E}|}$ 
8:   if  $\mathbf{y}_i$  has been successfully found then
9:      $\mathcal{D} \leftarrow \mathcal{D} \cup \{(\mathbf{x}_i, \mathbf{y}_i)\}$ 
10:  end if
11: end for
12: return  $\mathcal{D}$ 

```

Dong et al. 2020; Zamzam and Baker 2020; Canyasse, Dalal, and Mannor 2017; Chatzos, Mak, and Van Hentenryck 2021). Not all prior approaches consider regional/individual variations and not all prior approaches predict all the solution variables for ACOPF (i.e., $\dim(\mathbf{y}_i) < 2|\mathcal{G}| + |\mathcal{N}| + |\mathcal{E}|$). Some studies may only use simple uniform/Gaussian distributions for $\mathfrak{B}/\mathfrak{E}$.

2.4 Active Sampling

Active sampling (Angluin 1988; Lewis and Catlett 1994; Kumar and Gupta 2020; Ren et al. 2021) aims at finding a small set \mathcal{D} of data samples from a distribution \mathcal{D}_U to train a machine-learning model. In other words, given an unlabeled sample distribution \mathcal{D}_U , the goal of active sampling is to design a query strategy Q that chooses a small set of samples \mathcal{D} from \mathcal{D}_U to label. Let \mathbf{x} and \mathbf{y} be the vector of input and output features of a data sample, i.e., $(\mathbf{x}, \mathbf{y}) \in \mathcal{D}$, $h_{\mathcal{D}}$ be a learning model trained on data set \mathcal{D} , i.e., $h_{\mathcal{D}}(\mathbf{x}) = \hat{\mathbf{y}}$, and \mathbb{L} be a loss metric for measuring the prediction quality. The data set \mathcal{D}^* with the highest prediction accuracy is defined by a bilevel optimization problem:

$$\begin{aligned} \mathcal{D}^* \in \underset{\mathcal{D}}{\operatorname{argmin}} \quad & \mathbb{E}_{(\mathbf{x}, \mathbf{y}) \sim \mathcal{D}} [\mathbb{L}(h_{\mathcal{D}}^*(\mathbf{x}), \mathbf{y})] \\ \text{s.t.} \quad & h_{\mathcal{D}}^*(\mathbf{x}) \in \underset{h}{\operatorname{argmin}} \mathbb{E}_{(\mathbf{x}, \mathbf{y}) \in \mathcal{D}} [\mathbb{L}(h(\mathbf{x}), \mathbf{y})] \end{aligned} \quad (2)$$

Solving (2) optimally is challenging. For many applications, drawing samples incrementally during training is more computationally efficient. Let $\mathcal{D}^S = \operatorname{supp}(\mathcal{D}_U)$ be the support set of distribution \mathcal{D}_U . Acquisition functions α (or scoring functions (Choi et al. 2021)) are commonly used in active sampling applications to select the best k samples from \mathcal{D}^S for the next training cycle. The set \mathcal{D}_k^* containing the k best samples drawn with acquisition function α is defined as:

$$\mathcal{D}_k^* \in \underset{\mathcal{D}_k \subseteq \mathcal{D}^S \text{ s.t. } |\mathcal{D}_k|=k}{\operatorname{argmax}} \quad \alpha(\mathcal{D}_k) \quad (3)$$

Note that acquisition functions are usually customized per application, and may vary substantially from application to application. Many acquisition functions analyze/query the learning model h to select the next set \mathcal{D}_k^* for training.

3 Related Work

Most general active learning / sampling mechanisms (Wu 2018; Tsymbalov, Panov, and Shapeev 2018; Cai, Zhang, and Zhou 2013) label data samples based on acquisition scores of individual samples. Scores are often computed based on evaluations of the learning model, and the subset of samples with the highest scores will then be added to the data set. Some work also considers correlations between candidate input samples and/or ranking multiple *unlabeled* samples at the same time as a batch, e.g., BatchBALD (Kirsch, Van Amersfoort, and Gal 2019), and BADGE (Ash et al. 2019).

Contrary to prior approaches, ABS does not work at the level of individual samples: instead, it partitions the input distribution in various regions and determines, based on a dedicated validation set, which regions are in need of more samples. The validation set contains a list of buckets, where each bucket contains labeled validation samples for each individual partitioned subspace. ABS has several advantages: it exploits the structure of the underlying distribution, and it separates the analysis of the regions from the sampling process. In the context of optimization proxies, ABS also makes it possible to avoid generating infeasible inputs.

The effects of increasing learning rate during training have been the focus of several recent works including (Smith 2017; Smith and Topin 2019; Loshchilov and Hutter 2016; Zaheer et al. 2018). Most active learning approaches focus on decreasing the learning rate during training (Liu et al. 2021; Roy, Unmesh, and Namboodiri 2018). One of the novelties of ABS is to both *increase* and decrease the learning rate when appropriate. This allows ABS to avoid premature termination after adding a new batch of samples.

4 Active Learning for ACOPF

This section describes the novel active learning framework ABS. It first presents the Deep Neural Network (DNN) for ACOPF learning. It then introduces the core idea of ABS before going into the individual components in detail.

4.1 Active Learning: DNN Model

The ACOPF problem in Model 1 can be viewed as a high dimensional nonlinear function h_{ac} , taking input vectors for \mathbf{p}^d and \mathbf{q}^d , and returning optimal values for \mathbf{p}^g , \mathbf{q}^g , \mathbf{v} , and $\Delta\boldsymbol{\theta}$. The learning task for OPF typically generates a finite set \mathcal{D} of data samples, and each sample $(\mathbf{x}, \mathbf{y}) \in \mathcal{D}$ is of the form: $\mathbf{x} = (\mathbf{p}^d, \mathbf{q}^d)$, $\mathbf{y} = (\mathbf{p}^g, \mathbf{q}^g, \mathbf{v}, \Delta\boldsymbol{\theta})$. For ease of identification between samples, subscripts will be appended after \mathbf{x}/\mathbf{y} when there is no ambiguity, e.g., \mathbf{x}_i refers to the input features of the i^{th} sample.

This work uses Deep Neural Networks (DNNs) to illustrate the benefits of active learning for speeding up ACOPF learning. DNNs are composed of a sequence of layers, with each layer taking as input the results of the previous layer (e.g., (LeCun, Bengio, and Hinton 2015)). The function connecting the layers is given by $\mathbf{y} = \pi(\mathbf{W}\mathbf{x} + \mathbf{b})$, where $\mathbf{x} \in \mathbb{R}^n$, $\mathbf{y} \in \mathbb{R}^m$, $\mathbf{W} \in \mathbb{R}^{m \times n}$, $\mathbf{b} \in \mathbb{R}^m$, and π define the input vector, the output vector, the weight matrix, the bias vector, and the activation function. The framework

Algorithm 2 ABS: ACTIVE BUCKETIZED SAMPLING

Parameters: Initial learning rate β_0 ; Learning rate bounds $\bar{\beta}$ & β ; Patience thresholds $\bar{\rho}_1$ & $\bar{\rho}_2$; Learning rate factors γ_1 & γ_2

Termination condition: Time limit \bar{t}

Inputs: Initial data set \mathcal{D}_0 ; Bucket-validation set \mathcal{D}_V ; DNN h

Outputs: DNN h

```
1:  $\beta \leftarrow \beta_0, l_V^* \leftarrow \infty, \rho_1 \leftarrow 0, \rho_2 \leftarrow 0, \mathcal{D} \leftarrow \mathcal{D}_0,$   
2: while  $\text{RUNTIME}() < \bar{t}$  do  
     $\triangleright$  Training  
3:   for  $(\mathbf{x}_i, \mathbf{y}_i) \in \mathcal{D}$  do  
4:      $h \leftarrow \text{BACKPROP}(\mathbb{L}(h(\mathbf{x}_i), \mathbf{y}_i), \beta)$   
5:   end for  
     $\triangleright$  Validation & LR Update  
6:    $l_V \leftarrow \sum_{(\mathbf{x}_i, \mathbf{y}_i) \in \mathcal{D}_V} \mathbb{L}(h(\mathbf{x}_i), \mathbf{y}_i)$   
7:    $\rho_1, \rho_2, l_V^*, \beta \leftarrow \text{LR-UPDATE}(\rho_1, \rho_2, l_V, l_V^*, \beta)$   
     $\triangleright$  Active Sampling  
8:   if  $\rho_2 > \bar{\rho}_2$  then  
9:      $\mathcal{D} \leftarrow \mathcal{D} \cup \text{ACTIVESAMPLE}(h, \mathcal{D}_V)$   
10:  end if  
11: end while
```

uses a DNN h to approximate the high dimensional nonlinear function h_{AC} with varying $t \geq 2$ hidden layers:

$$\begin{aligned} \mathbf{h}^1 &= \pi(\mathbf{W}^1 \mathbf{x} + \mathbf{b}^1), \\ \mathbf{h}^j &= \pi(\mathbf{W}^j \mathbf{h}^{j-1} + \mathbf{b}^j), \quad \forall j \in \{2, 3, \dots, t\} \\ \mathbf{y} &= \pi(\mathbf{W}^{t+1} \mathbf{h}^t + \mathbf{b}^{t+1}) \end{aligned}$$

Learning h on a data set \mathcal{D} consists of finding all the weight matrices \mathbf{W}^j and bias vectors \mathbf{b}^j to make the output predictions $\hat{\mathbf{y}}_i$ close to the ground truth data \mathbf{y}_i for all $(\mathbf{x}_i, \mathbf{y}_i) \in \mathcal{D}$, with the quality being measured by a loss function \mathbb{L} .

4.2 The Active Learning Scheme ABS

Algorithm 2 depicts the main structure of ABS. The novel contributions are in the algorithms for active sampling and learning rate adjustment, which are presented next.

The algorithm receives an initial data set \mathcal{D}_0 , a bucket-validation data set \mathcal{D}_V , and an initialized DNN model h as inputs. The initial and bucket-validation data sets \mathcal{D}_0 and \mathcal{D}_V can be constructed from LOADPERTURB in Algorithm 1, or constructed from historically known ACOPF solutions. The bucket-validation data set allows ABS to decouple the sample generation from the assessment of where samples are needed. Line 1 initializes the routine variables including the learning rate, best validation loss, patience counters, and data sets. Lines 2 - 12 constitute the main loop of the training algorithm, which terminates when the total runtime $\text{RUNTIME}()$ exceeds its limit. Lines 3 - 5 constitute the training portion of the routine. For each data sample $(\mathbf{x}_i, \mathbf{y}_i)$, ABS computes the prediction loss $\mathbb{L}(h(\mathbf{x}_i), \mathbf{y}_i)$, then uses back-propagation BACKPROP to update the weights & biases for the DNN h . The first argument

Algorithm 3 ACTIVESAMPLE

Parameters: Acquisition function α ; Distributor function η ; Maximum number of new samples \bar{n}

Inputs: DNN h , Bucket-validation set \mathcal{D}_V

Output: Set of new samples \mathcal{D}^+

```
1: Partition bucket-validation data into a set of  $k$  buckets  
    $\{B_1, B_2, \dots, B_k\} \leftarrow \text{PARTITION}(\mathcal{D}_V)$   
2: Evaluate each bucket with acquisition function  $\alpha(\cdot)$   
    $\mathcal{S} = \{s_i : s_i \leftarrow \alpha(B_i), \forall i \in [1..k]\}$   
3: Compute samples to be drawn for each individual bucket,  
   with a score-based distributor function  $\eta(\cdot)$   
    $\mathcal{N} = \{n_1, n_2, \dots, n_k\} \leftarrow \eta(\mathcal{S}, \bar{n})$   
4: Sample  $n_i$  times for each bucket  $B_i$   
    $\mathcal{X}_i^+ \leftarrow \{\mathbf{x}_j : \mathbf{x}_j \sim \mathfrak{D}_{B_i}, \forall j \in [1, n_i]\}, \forall i \in [1..k]$   
5: Compute ACOPF solutions for new samples  $\mathcal{X}_i^+$   
    $\mathcal{Y}_i^+ \leftarrow \{\mathbf{y}_j : \mathbf{y}_j \leftarrow \text{ACOPF}(x_j), \forall j \in [1, n_i]\},$   
    $\forall i \in [1..k]$   
6: Construct & return  $\mathcal{D}^+$   
    $\mathcal{D}_i^+ = \{(\mathbf{x}_j, \mathbf{y}_j) : \mathbf{x}_j \in \mathcal{X}_i^+, \mathbf{y}_j \in \mathcal{Y}_i^+, \forall j \in [1, n_i]\}$   
    $\forall i \in [1..k]$   
    $\mathcal{D}^+ \leftarrow \bigcup_{i \in [1..k]} \mathcal{D}_i^+$ 
```

of BACKPROP expects a loss value, and the second argument takes in the learning rate. For simplicity, the algorithm ignores the mini-batch implementations and GPU routines to speed up the training process; these have been implemented and are used in the experimental results. Line 6 computes the validation loss from samples within the bucket-validation data set. Line 7 calls the LR-UPDATE routine (Algorithm 4) to update the patience counters ρ_1, ρ_2 , and the learning rate β . Finally, new samples will be drawn and their ACOPF will be computed (Lines 8 - 10) when the patience counter ρ_2 (updated by Algorithm 4) exceeds its threshold.

4.3 Bucketized-Active Sampling

Algorithm 3 presents the active sampling routine of ABS. There are two key innovations in ABS: (1) it decouples the assessment of where additional samples are needed from the sample generation and (2) it partitions the input distribution into regions (buckets) that capture the inherent structure of the application at hand. The first innovation is implemented through the use of dedicated validation set of samples (the bucket-validation set) that determine where samples are needed. In other words, instead of generating samples based on their *individual* qualities, ABS uses a pre-chosen set to determine the *regions* where samples are most needed. By comparing properties across different buckets, ABS effectively allocates computational resources to poorly performing regions, resulting in a more efficient sampling and learning routine. The general process is described next:

- **Step 1** partitions the bucket-validation data set into buckets. The partitioning routine can be based on the regional load level (i.e., $b_i \sim \mathfrak{B}$ from Algorithm 1), or simply based on the total active load demand in the network.
- **Step 2** evaluates the buckets using the acquisition function and returns a set \mathcal{S} with scores s_i for each bucket.

Each score $s_i \in \mathcal{S}$ reflects the urgency of new samples needed for each bucket i .

- **Step 3** uses a *distributor function* to decide how many samples to generate for every bucket based on the scores.
- **Step 4** generates the input feature vector \mathbf{x} of n_i new samples accordingly, from a predefined distribution \mathcal{D}_{B_i} for every bucket i . The distribution \mathcal{D}_{B_i} can be a projection of the original sampling distribution \mathcal{D}_U onto the domain/feasible space of B_i .
- **Step 5** computes the ACOPF solutions and records the required output features \mathbf{y} for every generated input feature vector \mathbf{x} across all the buckets.
- **Step 6** reconstructs the new samples and returns them to the main learning routine.

Acquisition Functions Step 2 of ABS requires an acquisition function α to evaluate & score each individual bucket B_i . In ABS, α evaluates data samples from B_i :

$$\alpha(B_i) \equiv \frac{1}{|B_i|} \sum_{(\mathbf{x}_j, \mathbf{y}_j) \in B_i} \mathbb{M}(h, \mathbf{x}_j, \mathbf{y}_j) \quad (4)$$

where \mathbb{M} is a function measuring the score of individual samples that has access to the weights & bias values of the training model, and every individual sample. ABS was evaluated on the following choices of acquisition metric \mathbb{M} :

1. **Loss Error (LE)**: $\mathbb{L}(h(\mathbf{x}_j), \mathbf{y}_j)$;
2. **Monte-Carlo Variance of Predictions (MCV-P)**: $\text{Var}\{h^1(\mathbf{x}_j), h^2(\mathbf{x}_j), \dots, h^\tau(\mathbf{x}_j)\}$, where each $h^i, i \in [1.. \tau]$ has a random dropout mask;
3. **Monte-Carlo Variance of Loss Errors (MCV-L)**: $\text{Var}\{\mathbb{L}(h^1(\mathbf{x}_j), \mathbf{y}_j), \mathbb{L}(h^2(\mathbf{x}_j), \mathbf{y}_j), \dots, \mathbb{L}(h^\tau(\mathbf{x}_j), \mathbf{y}_j)\}$, where each $h^i, i \in [1.. \tau]$ has a random dropout mask;
4. **Input Gradient (IG)**: the norm of the loss gradient w.r.t. the input, i.e., $\|\nabla_{\mathbf{x}} \mathbb{L}(h(\mathbf{x}_j), \mathbf{y}_j)\|$;
5. **Last-layer Gradient (LG)**: the norm of the loss gradient w.r.t. the last-layer neurons, i.e. $\|\nabla_{\mathbf{W}^{t+1}} \mathbb{L}(h(\mathbf{x}_j), \mathbf{y}_j)\|$.

Monte-Carlo Variance (MCV) metrics were used by prior approaches, e.g., in MCDUE (Tsymbolov, Panov, and Shapeev 2018). Gradient metrics are also widely adopted, e.g., BADGE (Ash et al. 2019).

Distributor Functions Step 3 of ABS requires a distributor function η to decide how to distribute the samples based on the scores computed by α . The framework requires η to return a set N satisfying $0 \leq \sum_{n_i \in N} n_i \leq \bar{n}$. ABS has been evaluated with two distributor functions $\eta(\mathcal{S}, \bar{n})$:

1. **Maximum distribution (MD)**¹:

$$\forall n_i \in N : n_i \equiv \begin{cases} \bar{n} & \text{if } i \in \text{argmax}_{j \in [1..k]} s_j, \\ 0 & \text{otherwise.} \end{cases}$$

2. **Proportion distribution (PD)**:

$$\forall n_i \in N : n_i \equiv \frac{\bar{n} s_i}{\sum_{s_j \in \mathcal{S}} s_j}$$

¹In case of a tie, argmax arbitrarily chooses one bucket.

Algorithm 4 LR-UPDATE($\rho_1, \rho_2, l_V, l_V^*, \beta$)

```

1: if  $l_V \geq l_V^*$  then
2:    $\rho_1 \leftarrow \rho_1 + 1, \rho_2 \leftarrow \rho_2 + 1$ 
3: else
4:    $l_V^* \leftarrow l_V, \rho_1 \leftarrow 0, \rho_2 \leftarrow 0$ 
5: end if
6: if  $\rho_1 > \bar{\rho}_1$  then
7:    $\beta \leftarrow \min\{\max\{\gamma_1 \beta, \underline{\beta}\}, \bar{\beta}\}$ 
8: end if
9: if  $\rho_2 > \bar{\rho}_2$  then
10:   $\beta \leftarrow \min\{\max\{\gamma_2 \beta, \underline{\beta}\}, \bar{\beta}\}$ 
11: end if
12: return:  $\rho_1, \rho_2, l_V^*, \beta$ 

```

4.4 Learning Rate Adjustment

Another novelty of ABS is its implementation of the learning rate adjustment, which is a significant extension of REDUCELRONPLATEAU (Paszke et al. 2019; Chollet et al. 2015). ABS uses two patience counters ρ_1 and ρ_2 . Counter ρ_1 is paired with γ_1 , the classical discount factor ($\gamma_1 < 1.0$), to reduce the learning rate β when ρ_1 reaches its threshold $\bar{\rho}_1$. In addition, to avoid premature learning convergence when new samples are added, ABS uses a boosting factor $\gamma_2 > 1.0$ to increase the learning rate when patience counter ρ_2 reaches its threshold $\bar{\rho}_2$. This avoids “local optima” (Gal, Islam, and Ghahramani 2017) without requiring re-initialization of weights after active sampling.

5 Experimental Evaluation

Experimental Setup The ACOPF data sets were computed using Julia with Ipopt (Biegler and Zavala 2009). The active learning procedures were implemented in Python with PyTorch (Paszke et al. 2019). The experimental results are presented for the PD distributor since it achieves better learning quality.

Benchmarks The experimental results are presented for two public benchmark networks 300_ieee and 1354_pegase from PGLib (Babaiejadsarookolae et al. 2019), as well as France-EHV, an industrial proprietary benchmark to showcase performance on real systems. Table 2 provides a summary of the three benchmarks. The evaluation uses Algorithm 1 to generate datasets with $\mathfrak{B} = \text{Uniform}(0.8, 1.2)$ and $\mathfrak{E} = \text{LogNormal}(0, 0.05)$, except France-EHV which has \mathfrak{B} set to $\text{Uniform}(0.6, 1.0)$.

Learning Models The experiments use fully connected DNNs with 3 - 5 hidden layers and sigmoid activation functions. Hidden layer dimensions are set to match the prediction feature size $2|\mathcal{G}| + |\mathcal{N}| + |\mathcal{E}|$. The training uses a mini-batch size of 128, a dropout rate of 15%, the AdamW optimizer (Loshchilov and Hutter 2018), and the L_1 norm as the loss function. 256 samples are initially labeled before training and 5000 testing samples are used for evaluations. Models are trained for at most 150 minutes. Results are re-

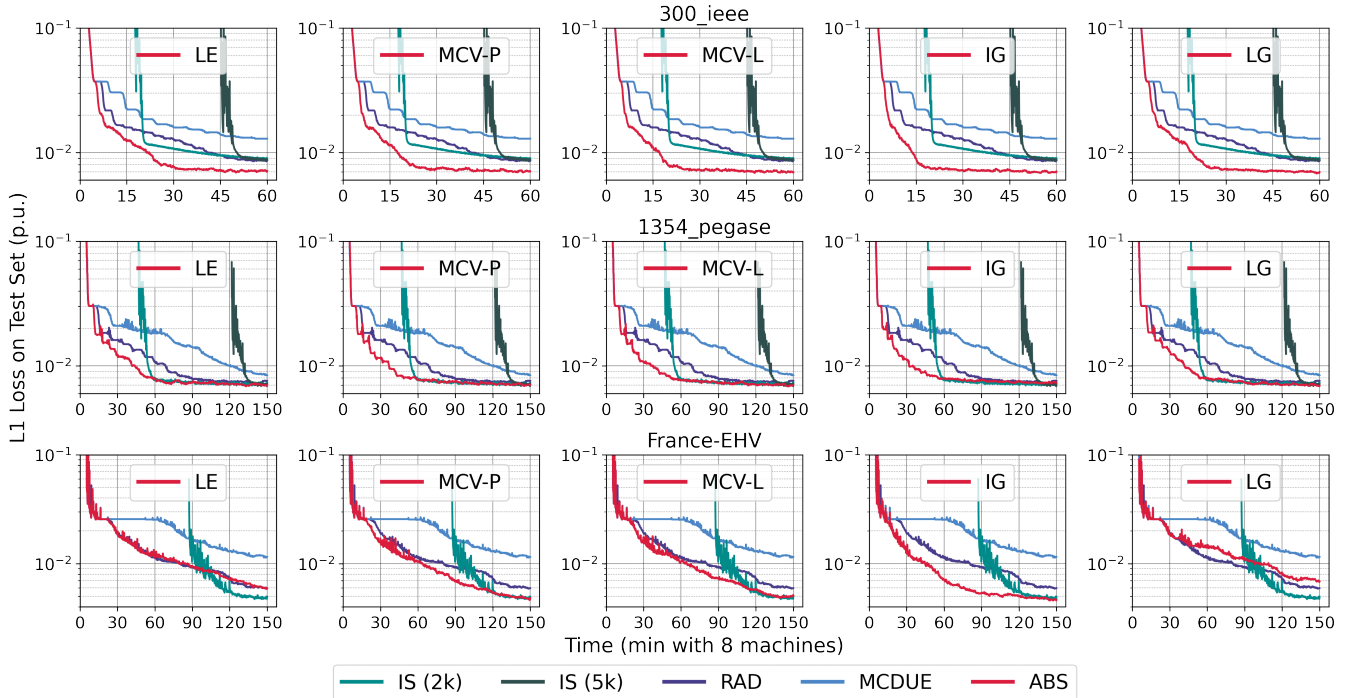


Figure 1: Mean L1 Loss on testing set, averaged across 50 trials.

| Benchmark Network | $ \mathcal{N} $ | $ \mathcal{L} $ | $ \mathcal{G} $ | $ \mathcal{E} $ |
|-------------------|-----------------|-----------------|-----------------|-----------------|
| 300_ieee | 300 | 201 | 69 | 411 |
| 1354_pegase | 1354 | 673 | 260 | 1991 |
| France-EHV | 1737 | 1731 | 290 | 2350 |

Table 2: Number of buses, loads, generators, and branches.

ported on the testing data set, and are averaged over 50 trials using different seeds.

Bucket-Validation Set Construction 1024 samples are first labeled using LOADPERTURB. Let $\bar{n}_V \leq 1024$ be the number of feasible samples, k be the desired number of buckets, and $b(d_i)$ be the load factor of data sample d_i . ABS partitions the feasible samples into k buckets, in ascending order of load factor, i.e., $\forall d_i \in B_i, d_j \in B_j, i < j : b(d_i) \leq b(d_j)$. All buckets of the bucket-validation set have $\lfloor \frac{\bar{n}_V}{k} \rfloor$ feasible samples except for the last bucket which may have less.

Baselines ABS is compared with three sampling methods:

1. Inactive Sampling (IS): the training data set is completely generated before training by sampling uniformly from the input domain.
2. Random Active Sampling (RAD): an active method that samples from the input domain uniformly.
3. Monte-Carlo Dropout Uncertainty Estimation (MCDUE): the state-of-the-art active sampling approach, selecting samples with the highest model uncertainty.

Inactive sampling is used to show the benefits of sampling data actively. MCDUE is a state-of-the-art method in active learning, with the number of trials $\tau = 25$ as in (Tsybalov, Panov, and Shapeev 2018). At every iteration, a pool of 5000 unlabeled samples is generated uniformly from the input domain for MCDUE to select from.

Learning Quality: Accuracy & Convergence Figure 1 presents the prediction accuracy (L1-loss) over the training period. Each row corresponds to a different grid, and each column corresponds to a different acquisition function. Overall, the prediction accuracy of ABS is consistently better than the other approaches. Both RAD and MCDUE take significantly more time to match the level of accuracy of ABS. Even though classic generate-then-train (IS) approaches may converge faster, they suffer from the significant amount of time needed to pre-generate data samples. Observe also that ABS-IG consistently has the lowest prediction errors over the training horizon. Interestingly, MCV-P, MCV-L, and IG converge faster than LE and LG. Figure 3 shows the constraint violation for ABS-IG over the same training period. Again, ABS-IG outperforms other approaches, except for France-EHV and 2 hours of training time, where IS-2k has fewer violations.

Sampling Behavior of Acquisition Functions Figure 2 shows the distribution of samples, explaining why ABS-IG is most effective. Observe the fundamentally different sampling behavior of IG compared to the other acquisition functions. LE, MCV-P, and MCV-L have no clear preferences across buckets (except in the higher ranges of base loads, which will be discussed shortly), reducing the benefits of

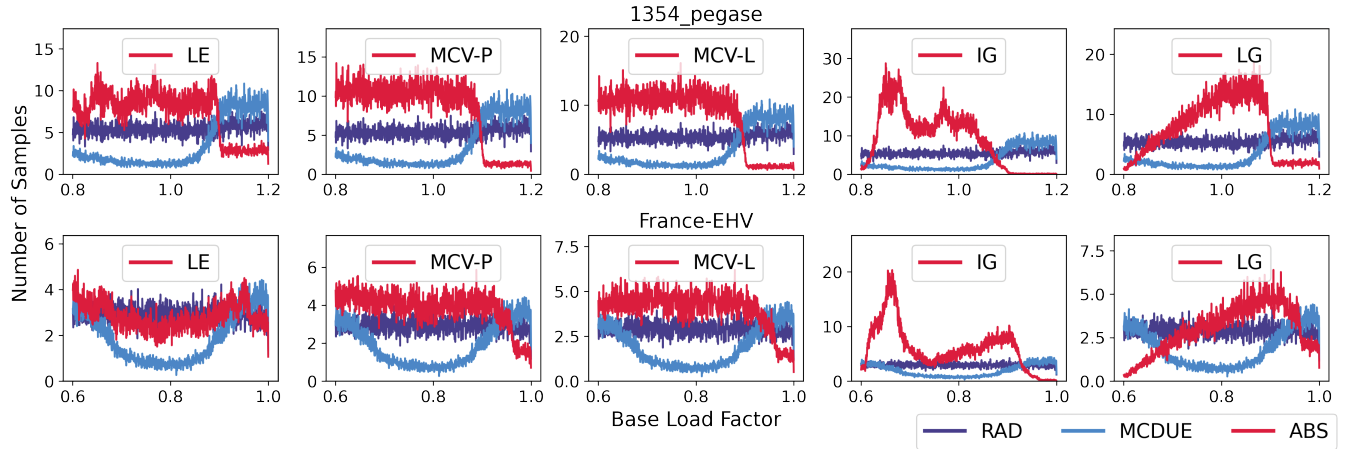


Figure 2: Mean sampling distributions across 50 trials. 300_ieee results are included in the appendix.

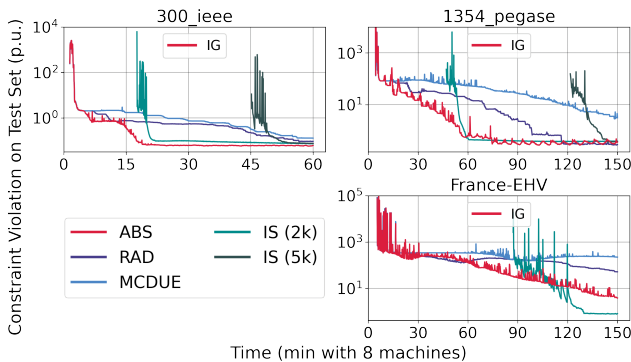


Figure 3: Mean constraint violations for ABS-IG

active learning. LG has a clear bias towards samples with higher base loads, as it uses the gradient of the loss with respect to the last layer. In contrast, IG has a much more differentiated sampling pattern. Because it uses the gradient of loss with respect to the input features, *IG isolates highly sensitive regions of the input space*. These samples trigger significant weight updates, even after passing through *all the DNN layers* during back-propagation. Thus, IG captures information from both forward evaluations and backward propagations. LE, MCV-P, and MCV-L mostly capture forward-information (prediction and loss), and fail to differentiate the behavior of different regions. LG has too large a bias towards samples with larger output values.

Second, observe that all acquisition functions under-sample regions with high load factor (e.g., >1.1 for 1354_pegase), contrary to MCDUE. These regions contain many infeasible samples which are not realistic as they correspond to loads that are over either global or regional production capabilities. Uncertainty-based active sampling methods (e.g., MCDUE) select samples with the highest predictive variance, which often correspond to infeasible samples. In contrast, the bucket-validation set allows ABS to allocate computational resources efficiently by surgically sam-

| | 1354_pegase | | France-EHV | |
|-------|-------------|------------|-------------|------------|
| | Feasible | Infeasible | Feasible | Infeasible |
| RAD | 3937 | 1477 | 2651 | 266 |
| MCDUE | 1455 | 2078 | 1554 | 334 |
| LE | 6306 | 887 | 2556 | 274 |
| MCV-P | 7519 | 533 | 3621 | 214 |
| MCV-L | 7723 | 483 | 3794 | 203 |
| IG | 8860 | 135 | 5802 | 104 |
| LG | 6709 | 758 | 2718 | 264 |

Table 3: Mean number of samples generated across 50 trials.

pling in feasibility-dense regions, which are more useful for learning. Table 3 highlights these observations further and shows that ABS-IG is also able to label many more samples within the allocated time, limiting the number of time-consuming infeasible samples and focusing on regions of the input space that are more sensitive but whose samples are typically cheaper to label.

6 Conclusion & Future Work

This paper proposed ABS, a novel bucketized active learning framework. The framework partitions the input distribution into buckets and labels data samples based on the bucketized input space. A key innovation of ABS is the use of a bucket-validation set to decide where new samples are needed, decoupling the decision about where to sample from the actual sample generation. ABS also adopts a new learning rate adjustment scheme, and incorporates multiple acquisition functions inspired by the literature. Experimental evaluation against state-of-the-art approaches indicates the superior performance of ABS on large ACOF benchmarks. Future work to improve ABS includes dynamic schemes for the selection of validation sets and bucket partitioning, and cost-aware active sampling approaches.

Acknowledgements

This research is partly funded by NSF Awards 1912244 and 2112533, and ARPA-E Perform Award AR0001136.

References

- Angluin, D. 1988. Queries and Concept Learning. *Machine Learning*, 2(4): 319–342.
- Ash, J. T.; Zhang, C.; Krishnamurthy, A.; Langford, J.; and Agarwal, A. 2019. Deep Batch Active Learning by Diverse, Uncertain Gradient Lower Bounds. In *7th International Conference on Learning Representations (ICLR 2019)*.
- Babaeinejadsarookolae, S.; Birchfield, A.; Christie, R. D.; Coffrin, C.; DeMarco, C.; Diao, R.; Ferris, M.; Fliscounakis, S.; Greene, S.; Huang, R.; Jozs, C.; Korab, R.; Lesieutre, B.; Maeght, J.; Mak, T. W. K.; Molzahn, D. K.; Overbye, T. J.; Panciatici, P.; Park, B.; Snodgrass, J.; Tbaileh, A.; Van Hentenryck, P.; and Zimmerman, R. 2019. The Power Grid Library for Benchmarking AC Optimal Power Flow Algorithms. arXiv:1908.02788.
- Baker, K. 2020. A Learning-Boosted Quasi-Newton Method for AC Optimal Power Flow. In *Advances in Neural Information Processing Systems 33 (NeurIPS 2020)*.
- Baran, M. E.; and Wu, F. F. 1989. Optimal Capacitor Placement on Radial Distribution Systems. *IEEE Transactions on Power Delivery (PWRD)*, 4(1): 725–734.
- Biegler, L. T.; and Zavala, V. M. 2009. Large-Scale Nonlinear Programming Using Ipopt: An Integrating Framework for Enterprise-wide Dynamic Optimization. *Computers & Chemical Engineering*, 33(3): 575–582.
- Cai, W.; Zhang, Y.; and Zhou, J. 2013. Maximizing Expected Model Change for Active Learning in Regression. In *13th IEEE International Conference on Data Mining (ICDM 2013)*, 51–60. IEEE.
- Cain, M. B.; O’neill, R. P.; Castillo, A.; et al. 2012. History of Optimal Power Flow and Formulations. *Federal Energy Regulatory Commission (FERC)*, 1: 1–36.
- Canyasse, R.; Dalal, G.; and Mannor, S. 2017. Supervised Learning for Optimal Power Flow as a Real-time Proxy. In *8th IEEE Conference on Power & Energy Society Innovative Smart Grid Technologies (ISGT 2017)*, 1–5. IEEE.
- Chatzos, M.; Mak, T. W.; and Van Hentenryck, P. 2021. Spatial Network Decomposition for Fast and Scalable AC-OPF Learning. *IEEE Transactions on Power Systems (TPWRS)*.
- Chen, W.; Park, S.; Tanneau, M.; and Van Hentenryck, P. 2022. Learning Optimization Proxies for Large-Scale Security-Constrained Economic Dispatch. *Electric Power Systems Research*, 213: 108566.
- Choi, J.; Elezi, I.; Lee, H.-J.; Farabet, C.; and Alvarez, J. M. 2021. Active Learning for Deep Object Detection via Probabilistic Modeling. In *2019 IEEE/CVF International Conference on Computer Vision (ICCV)*, 10264–10273.
- Chollet, F.; et al. 2015. Keras. <https://keras.io>.
- Diehl, F. 2019. Warm-Starting AC Optimal Power Flow With Graph Neural Networks. In *Advances in Neural Information Processing Systems 32 (NeurIPS 2019)*, 1–6.
- Dong, W.; Xie, Z.; Kestor, G.; and Li, D. 2020. Smart-PGSim: Using Neural Network to Accelerate AC-OPF Power Grid Simulation. In *2020 International Conference for High Performance Computing, Networking, Storage and Analysis (SC20)*, 1–15. IEEE.
- Fioretto, F.; Mak, T. W.; and Van Hentenryck, P. 2020. Predicting AC Optimal Power Flows: Combining Deep Learning and Lagrangian Dual Methods. In *34th AAAI Conference on Artificial Intelligence (AAAI-20)*, 630–637.
- Fisher, E. B.; O’Neill, R. P.; and Ferris, M. C. 2008. Optimal Transmission Switching. *IEEE Transactions on Power Systems (TPWRS)*, 23(3): 1346–1355.
- Gal, Y.; Islam, R.; and Ghahramani, Z. 2017. Deep Bayesian Active Learning With Image Data. In *34th International Conference on Machine Learning (ICML 2017)*, 1183–1192. PMLR.
- Guha, N.; Wang, Z.; Wytock, M.; and Majumdar, A. 2019. Machine Learning for AC Optimal Power Flow. In *36th International Conference on Machine Learning (ICML 2019)*.
- Kirsch, A.; Van Amersfoort, J.; and Gal, Y. 2019. Batch-BALD: Efficient and Diverse Batch Acquisition for Deep Bayesian Active Learning. *Advances in Neural Information Processing Systems 32 (NeurIPS 2019)*, 32.
- Kumar, P.; and Gupta, A. 2020. Active Learning Query Strategies for Classification, Regression, and Clustering: A Survey. *Journal of Computer Science and Technology*, 35(4): 913–945.
- LeCun, Y.; Bengio, Y.; and Hinton, G. 2015. Deep Learning. *Nature*, 521(7553): 436–444.
- Lewis, D. D.; and Catlett, J. 1994. Heterogeneous Uncertainty Sampling for Supervised Learning. In *Machine Learning Proceedings 1994: Proceedings of the Eighth International Conference*, 148. Morgan Kaufmann.
- Liu, Z.; Ding, H.; Zhong, H.; Li, W.; Dai, J.; and He, C. 2021. Influence Selection for Active Learning. In *2021 IEEE/CVF International Conference on Computer Vision (ICCV)*, 9274–9283.
- Loshchilov, I.; and Hutter, F. 2016. SGDR: Stochastic Gradient Descent With Warm Restarts. *Learning*, 10: 3.
- Loshchilov, I.; and Hutter, F. 2018. Decoupled Weight Decay Regularization. In *6th International Conference on Learning Representations (ICLR 2018)*.
- Owerko, D.; Gama, F.; and Ribeiro, A. 2020. Optimal Power Flow Using Graph Neural Networks. In *2020 IEEE International Conference on Acoustics, Speech and Signal Processing (ICASSP)*, 5930–5934. IEEE.
- Pan, X.; Chen, M.; Zhao, T.; and Low, S. H. 2020. Deep-OPF: A Feasibility-Optimized Deep Neural Network Approach for AC Optimal Power Flow Problems. In *10th IEEE International Conference on Communications, Control, and Computing Technologies for Smart Grids (SmartGridComm 2019)*.
- Pan, X.; Zhao, T.; and Chen, M. 2019. DeepOPF: Deep Neural Network for DC Optimal Power Flow. In *10th IEEE International Conference on Communications, Control, and Computing Technologies for Smart Grids (SmartGridComm 2019)*, 1–6.

- Paszke, A.; Gross, S.; Massa, F.; Lerer, A.; Bradbury, J.; Chanan, G.; Killeen, T.; Lin, Z.; Gimelshein, N.; Antiga, L.; Desmaison, A.; Kopf, A.; Yang, E.; DeVito, Z.; Raison, M.; Tejani, A.; Chilamkurthy, S.; Steiner, B.; Fang, L.; Bai, J.; and Chintala, S. 2019. PyTorch: An Imperative Style, High-Performance Deep Learning Library. In Wallach, H.; Larochelle, H.; Beygelzimer, A.; d'Alché Buc, F.; Fox, E.; and Garnett, R., eds., *Advances in Neural Information Processing Systems 32 (NeurIPS 2019)*, 8024–8035. Curran Associates, Inc.
- Ren, P.; Xiao, Y.; Chang, X.; Huang, P.-Y.; Li, Z.; Gupta, B. B.; Chen, X.; and Wang, X. 2021. A Survey of Deep Active Learning. *ACM Computing Surveys (CSUR)*, 54(9): 1–40.
- Roy, S.; Unmesh, A.; and Namboodiri, V. P. 2018. Deep Active Learning for Object Detection. In *29th British Machine Vision Conference (BMVC 2018)*, 91.
- Smith, L. N. 2017. Cyclical Learning Rates for Training Neural Networks. In *2017 IEEE Winter Conference on Applications of Computer Vision (WACV)*, 464–472. IEEE.
- Smith, L. N.; and Topin, N. 2019. Super-Convergence: Very Fast Training of Neural Networks Using Large Learning Rates. In *Artificial Intelligence and Machine Learning for Multi-Domain Operations Applications*, volume 11006, 1100612. International Society for Optics and Photonics.
- Sun, X.; Luh, P. B.; Bragin, M. A.; Chen, Y.; Wang, F.; and Wan, J. 2017. A Decomposition and Coordination Approach for Large-Scale Security Constrained Unit Commitment Problems With Combined Cycle Units. In *IEEE Power & Energy Society General Meeting*, 1–5.
- Tam, S. 2011. Real-Time Security-Constrained Economic Dispatch and Commitment in the PJM: Experiences and Challenges. In *FERC Software Conference*.
- Tang, H.; Wang, S.; Chang, K.; and Guan, J. 2021. Intraday Dynamic Optimal Dispatch for Power System Based on Deep Q-Learning. *IEEJ Transactions on Electrical and Electronic Engineering*, 16(7): 954–964.
- Tang, Y.; Dvijotham, K.; and Low, S. 2017. Real-Time Optimal Power Flow. *IEEE Transactions on Smart Grid*, 8(6): 2963–2973.
- Tsymbalov, E.; Panov, M.; and Shapeev, A. 2018. Dropout-based Active Learning for Regression. In *7th International Conference on Analysis of Images, Social Networks and Texts (AIST 2018)*, 247–258. Springer.
- Verma, S.; Mukherjee, V.; et al. 2016. Transmission expansion planning: A review. In *3rd International Conference on Energy Efficient Technologies for Sustainability (ICEETS 2016)*, 350–355. IEEE.
- Wu, D. 2018. Pool-Based Sequential Active Learning for Regression. *IEEE Transactions on Neural Networks and Learning Systems*, 30(5): 1348–1359.
- Yan, Z.; and Xu, Y. 2020. Real-Time Optimal Power Flow: A Lagrangian Based Deep Reinforcement Learning Approach. *IEEE Transactions on Power Systems (TPWRS)*, 35(4): 3270–3273.
- Yu, T.; Liu, J.; Chan, K. W.; and Wang, J. 2012. Distributed Multi-Step Q (λ) Learning for Optimal Power Flow of Large-Scale Power Grids. *International Journal of Electrical Power & Energy Systems*, 42(1): 614–620.
- Zaheer, M.; Reddi, S.; Sachan, D.; Kale, S.; and Kumar, S. 2018. Adaptive Methods for Nonconvex Optimization. *Advances in Neural Information Processing Systems 31 (NeurIPS 2018)*, 31.
- Zamzam, A. S.; and Baker, K. 2020. Learning Optimal Solutions for Extremely Fast AC Optimal Power Flow. In *11th IEEE International Conference on Communications, Control, and Computing Technologies for Smart Grids (Smart-GridComm 2020)*, 1–6. IEEE.